

TUW - 95 - 23

PITHA - 95/24

gr-qc/9511081

Classical and Quantum Gravity in 1+1 Dimensions

Part II: The Universal Coverings

THOMAS KLÖSCH*

Institut für Theoretische Physik
Technische Universität Wien
Wiedner Hauptstr. 8-10, A-1040 Vienna
Austria

THOMAS STROBL†

Institut für Theoretische Physik
RWTH-Aachen
Sommerfeldstr. 26-28, D52056 Aachen
Germany

Abstract

A set of simple rules for constructing the maximal (e.g. analytic) extensions for any metric with a Killing field in an (effectively) two-dimensional spacetime is formulated. The application of these rules is extremely straightforward, as is demonstrated at various examples and illustrated with numerous figures. Despite the resulting simplicity we also comment on some subtleties concerning the concept of Penrose diagrams. Most noteworthy among these, maybe, is that (smooth) spacetimes which have both degenerate and non-degenerate (Killing) horizons do not allow for globally smooth Penrose diagrams. Physically speaking this obstruction corresponds to an infinite relative red/blueshift between observers moving across the two horizons. – The present work provides a further step in the classification of all global solutions of the general class of two-dimensional gravity-Yang-Mills systems introduced in Part I [1], comprising, e.g., all generalized (linear and nonlinear) dilaton theories. In Part I we constructed the local solutions, which were found to always have a Killing field; in this paper we provide all universal covering solutions (the simply connected maximally extended spacetimes). A subsequent Part III [2] will treat the diffeomorphism inequivalent solutions for all other spacetime topologies.

Part II is kept entirely self-contained; a prior reading of Part I is not necessary.

to appear in *Class. Quantum Grav.*

November 1995

*e-mail: kloesch@tph.tuwien.ac.at

†e-mail: tstrobl@physik.rwth-aachen.de

1 Introduction

As is well known, in two spacetime dimensions any metric is conformally flat: Using null coordinates u and v , g takes the form (conformal gauge)

$$g = \exp[\rho(u, v)] dudv . \quad (1)$$

So, at first sight it might appear that the causal structure of any 2d metric is the same as the one of a flat metric. Certainly this is far from true, as is seen from the various models of dilaton gravity or already from spherically symmetric 4d gravity. In many cases the nontrivial global structure comes about, because the (maximal) domain of definition of the function ρ in (1) is only a subset of \mathbb{R}^2 . For the (spherically reduced) Schwarzschild solution this is a well-known feature of the Kruskal coordinates; for Reissner-Nordström, or more complicated 2d metrics, the same mechanism applies in a less trivial way. Sometimes, moreover, it is not possible to stay within one plane sheet; the conformal gauge can only be achieved by allowing overlapping layers (cf. Fig. 6). And even within one sheet smoothness considerations may obstruct a global attainability of (1) (cf. Fig. 3). Thus, the global causal structure of general 1+1 metrics may be quite involved, even if, as in the present paper, attention is restricted to 1+1 metrics with Killing vectors.

Somewhat less popular than the conformal gauge (1), but for some purposes better suited, is the chiral gauge

$$g = 2dx^0dx^1 + k(x^0, x^1) dx^1dx^1 . \quad (2)$$

It results upon the choice of x^1 as a label for one set of null-lines and of x^0 as an appropriately normalized affine parameter on them; the normalization (or synchronization) of the affine parameters may be prescribed on any line $x^0 = c = const$ by requiring that there the “speeds” $\partial_0|_{c,x^1}$ have unit inner product with ∂_1 . Equivalently: Choose x^1 as above and subsequently, with these “provisional” coordinates, x^0 as $\int g_{01}(\tilde{x}^0, x^1)d\tilde{x}^0$.

If k in (2) does not depend on x^1 , this metric has a Killing field ∂_1 . But, remarkably, also the converse is true: *Any* 2d metric with a Killing vector allows for coordinates such that locally it takes the generalized Eddington-Finkelstein form

$$g = 2dx^0dx^1 + h(x^0)(dx^1)^2 . \quad (3)$$

It is obtained by labelling Killing trajectories and (locally) transversal null-lines by x^0 and x^1 , respectively, where x^1 is the Killing-flow parameter and x^0 an affine parameter of the chosen null-lines normalized as before. To arrive at (3) one can repeat the construction of (2), but now choosing $x^0 = c$ to be a Killing trajectory and x^1 a Killing-flow parameter along this line. For a given metric g the function h in (3) is generically unique up to an equivalence relation $h(x^0) \sim \frac{1}{a^2}h(ax^0 + b)$, $a, b = const$. Only for Minkowski and deSitter space this is not quite true, because they have more than one Killing field (in fact three). Minkowski space can be described by $h = ax^0 + b$ and (anti-)deSitter space of curvature R by $h = \frac{R}{2}(x^0)^2 + ax^0 + b$ (since $R \equiv h''$).¹

¹Different choices of $h(x^0)$ correspond to different Killing fields ∂_1 . For instance, in the case of Minkowski space $h = const$ implies that ∂_1 generates translations (timelike, null, or spacelike, according to $\text{sgn } h$), whereas h linear in x^0 ($a \neq 0$) corresponds to boosts. For deSitter cf. the paragraph around (10) and Fig. 9.

Our motivation for studying 2d spacetimes with a Killing field is that metrics of such a type arise in the analysis of the very general class of 2d gravity-Yang-Mills systems introduced in Part I [1] (cf. also Sec. 2): All the solutions of, e.g., generalized (linear or nonlinear) dilaton theory have a Killing field. This continues to hold for generalizations with nontrivial torsion as well as for a dynamical (possibly dilaton dependent) coupling of these theories to a Yang-Mills field of an arbitrary gauge group. In all of these cases we brought the metric g into the form (3) and determined the possible functions h . For any fixed pure gravity theory there is a one parameter family of such functions h (generalized Birkhoff theorem) while in the presence of a Yang-Mills field a second parameter arises. In the space of all possible Lagrangians considered in Part I, furthermore, any function h can be generated.

Clearly, in general a coordinate system (3) is attainable locally only. For instance, the Killing trajectories $x^0 = \text{const}$ may become parallel to the null-lines $x^1 = \text{const}$ somewhere or they may run into a point where the Killing vector field vanishes. In contrast to the more general charts (2), by construction (3) is applicable only in the neighbourhood of points where the Killing vector does not vanish. (We constructed a chart valid around points of vanishing Killing vector, too, cf. Eq. (9) below; but again, in general also these charts are local only). For physical reasons, however, one is interested in maximally extended spacetimes: All extremals (which, if timelike, describe the motion of test particles) should be either complete (have infinite length) or run into a true curvature singularity.

Thus, in the present paper, we will study the maximal extension of the local charts (3). Certainly, in general such an extension is not unique. Already the (analytic) Minkowski solution, $h \equiv 0$, allows for inextendible manifolds of planar, cylindrical, or toroidal topology (the latter two even carrying further continuous parameters). The Minkowski-plane, however, is the unique universal covering space of the cylinders and tori and they, vice-versa, are obtained by factoring out a discrete symmetry group from this covering manifold. This generalizes: Any multiply connected solution, however complicated it may be, can be obtained from the universal coverings (i.e. the maximally extended *simply connected* manifolds) by factoring out a discrete symmetry group (cf., e.g., [3]). Therefore, in the present paper we will restrict ourselves to the simply connected extensions. The global solutions with non-trivial spacetime topology will be dealt with then in the following paper [2].

Still even if we restrict ourselves to simply connected spacetimes the extension of a local solution of the form (3) is not unique without additional specifications. Take, e.g., the case that the function h is given in the interval $[0, 1]$ and known to vanish there. Obviously already within a chart of the type (3) there is an infinity of smooth extensions of the function h to values of x^0 outside the given interval. But even if the function h is known on a maximal domain of x^0 , having a boundary only if there $h'' \equiv R \rightarrow \pm\infty$, there are similar ambiguities in a smooth extension of the (generically) local chart (3) into regions not covered by that chart. One way to avoid such ambiguities is to require that g should be analytic everywhere. Alternatively, working in the framework of a given gravity-Yang-Mills model considered in Part I, we may require the field equations of the given Lagrangian to restrict the extension. In this case the universal covering solutions turn out to be unique also for non-analytic functions h . Either of these two philosophies underlies the simple extension rules derived in the present paper.

The organization of this paper is as follows: In Sec. 2 we recollect some of the results of Part I. This section serves mainly to recall the generality of models treated by us as well as to provide some explicit examples used later on for illustration. It may well be omitted on a first reading, if one is not so much interested in 1+1 gravity models but merely in the, say analytic, extension of a metric (3). In Sec. 3, then, we discuss some general properties of the metric (3) and use its symmetries to solve the equation of extremals.

Sections 4 and 5 are the heart of the present paper: Here we derive a simple building block principle for obtaining the universal covering solutions of any metric with local form (3). In the first of these two sections the charts underlying (3) are mapped into a finite subdomain of \mathbb{R}^2 with null-lines as Cartesian coordinates. These are the basic building blocks for Penrose diagrams, which are glued together in Section 5. The considerations are described by means of an illustration for a typical function h , cf. Figs. 2 and 5. Our method is a streamlined and generalized version of the one suggested previously by M. Walker [4] (cf. also [5]) for a rather restricted class of metrics. Also we point out some possible pitfalls within this method (ignored for the most part in the previous literature). The most severe one is that given a function h with zeros of different orders, despite the existence of a smooth inextendible covering space there is, in this case, *no* globally smooth Penrose diagram for it. The physical reason for such an obstruction is found in an infinite red/blue-shift (Fig. 3). Another issue concerns the boundary lines of Penrose diagrams. While any single space- or time-like boundary line may be straightened by a conformal diffeomorphism, in some cases it is again global smoothness that forbids to perform this operation to all boundary lines of a Penrose diagram at the same time, thus leaving some of these boundary lines bent out- or inwards (Figs. 4,7,11).

The resulting method to construct Penrose diagrams for a given metric (3) is summarized in terms of simple rules in Sec. 6. The list of rules is followed by their application to the three examples provided at the end of Sec. 2. This demonstrates the efficiency of the method. In its final form one merely has to determine the number and degrees of the zeros of the function h as well as its asymptotic behaviour. The rest is simple pictorial gluing.

On the level of purely local considerations the models considered in Part I show many similarities. However, taking global aspects into account, there arise relevant differences. This becomes particularly pronounced, when solutions on non-simply connected spacetimes are constructed (cf. Part III [2]). We give a first flavour of this in the concluding Sec. 7 and comment on related issues relevant for the quantum theory (Part IV [2]).

2 Recollection of Results of Part I

The model we deal with reads in its most general form

$$L = \int_M \left[X_a D e^a + X^3 d\omega + W(X_a X^a, X^3) \varepsilon \right] + \int_M Z(X_a X^a, X^3) \text{tr} (F \wedge *F) , \quad (4)$$

consisting of a gravity- and a Yang-Mills part. Here e^a with $a \in \{+, -\}$ is the zweibein in a light cone basis of the frame bundle, $\varepsilon \equiv e^- \wedge e^+$ is the corresponding volume form ($\Rightarrow \varepsilon^{+-} = +1$), and ω (or $\omega^a_b \equiv \varepsilon^a_b \omega$) is the Lorentz or spin connection; so $d\omega$ is the gravity curvature two-form and $D e^a \equiv d e^a + \varepsilon^a_b \omega \wedge e^b$ the torsion two-form. F is the curvature

two-form of the Yang-Mills gauge fields, the trace represents some non-degenerate inner product on the Lie algebra, and the Hodge dual operation “ $*$ ” is performed by means of the volume form ε . X^a and X^3 are dilaton-like dynamical fields, which in the Hamiltonian formulation will serve as momenta to the one-components of e^a , ω , respectively (cf. Part IV [2]). W and Z are some arbitrary potentials (with $Z \neq 0$ or $Z \equiv 0$) of X^3 and the Lorentz-invariant combination $X_a X^a \equiv 2X^+ X^-$. In the formulation above the metric g is obtained via $g = 2e^- e^+ \equiv e^- \otimes e^+ + e^+ \otimes e^-$.

The action (4) allows also to treat generalized 2d dilaton gravity [6] coupled to Yang-Mills fields:

$$L^{gdilYM} = \int_M d^2x \sqrt{-\det g} \left[D(\Phi)R + \frac{1}{2}g^{\mu\nu} \partial_\mu \Phi \partial_\nu \Phi - U(\Phi) + B(\Phi) \text{tr} F_{\mu\nu} F^{\mu\nu} \right], \quad (5)$$

where R is the Ricci scalar of g and Φ is the dilaton field. In order to describe (5) by means of the general action (4), however, e^a is no longer the standard zweibein; rather, now

$$g = K(X^3) e^+ e^- \quad (6)$$

where the conformal factor K is determined by the potential D in (5) (for further details cf. Part I). In this case $X^3 = D(\Phi)$, furthermore, and W and Z in (4) are X^a -independent so that the X^a -fields become Lagrange multiplier fields enforcing torsion zero (this holds also despite the complication (6)). We note on this occasion that for the same reasons as those given in the introduction the transformation (6), although conformal, has in some cases implications on the global causal structure of g (cf. related remarks in Part I as well as [7]). In contrast to minimally coupled massless scalar fields, furthermore, the Yang-Mills fields “feel” the conformal factor of the metric.

Let us make a side-remark: Obviously, in the transition from (5) to (4) one of the three potentials went into the redefinition of field variables (into (6) and/or $X^3 = D(\Phi)$). As shown implicitly in Part I, further field redefinitions allow to eliminate also these remaining two potentials in (4), reducing the action effectively to the one for a set of free abelian gauge fields. (Just implement the transformation to Casimir-Darboux coordinates, $X^a, X^3 \rightarrow \tilde{X}^i$ etc., on the level of the Lagrangian, cf., e.g., [8]). Such a procedure is legitimate, if one is interested in *local* solutions only, which, as in the present paper, are then extended to global ones by patching. This allows us to drop also the restriction $D' \neq 0$, made in Part I. On any of the branches of D with $D' \neq 0$ the transition from (5) to (4) is legitimate and the latter Lagrangian (or the further simplified version mentioned above) describes the corresponding local solutions perfectly well. However, when discussing the quantum theory of (5) via the formulation (4) in Part IV, the restriction $D' \neq 0$ (everywhere) may be essential.

In Part I it was shown that for the general class of models described by (4) or (5) nearly everywhere the local solution for g may be put into the form (3) with $h(x^0)$ as specified there. E.g. for (4) without Yang-Mills fields (i.e. $Z(X_a X^a, X^3) \equiv 0$) and without torsion (i.e. $W(X_a X^a, X^3) \equiv V(X^3)/2$), we found

$$h(x^0) = \int^{x^0} V(z) dz + C, \quad (7)$$

where the ‘‘Casimir constant’’ C is a meaningful constant of integration (related to the total mass). While in this case the free parameter C merely shifts h ‘‘vertically’’, the dependence on this parameter becomes more involved for theories with torsion or in the context of (5, 6). In the presence of Yang-Mills fields h depends on a second parameter, the ‘‘charge’’ $q = Z^2 \text{tr}(*F)^2 = \text{const.}$ Let us note (cf. Part I), furthermore, that the gravitational sector of any gravity-Yang-Mills system (4) may be described equivalently through (4) with potentials

$$\widetilde{W} := W + \frac{q}{Z}, \quad \widetilde{Z} := 0, \quad (8)$$

now to be analyzed for all possible values of q . Thus in particular a minimally coupled ($Z \equiv \text{const.}$) gauge field contributes to the metric g merely via a dynamical cosmological constant. Taking all the Yang-Mills potentials into account, on the other hand, the local solutions have been found to be parametrized by $r - 1$ further constants besides C and q , where r denotes the rank of the Lie algebra.

In the chiral gauge (3) also the other fields depend only on the coordinate x^0 so that ∂_1 generates symmetries of the full solutions to the field equations. In the case of (7), e.g., $X^3 = x^0$ and $X_a X^a = h(x^0)$. Generally, the coordinate x^0 in (3) always either ranges over all of \mathbb{R} or, if not, then on the boundary X^3 (or some ‘‘back-transformed’’ dilaton field) diverges.²

The chart (3) only fails at zeros of the Killing field. For isolated simple zeros (say, at $x^0 = a$) we have already in Part I ([1], Eqs. (64,65)) obtained the chart

$$g = -\frac{4}{h'(a)} \left[dx dy + \frac{xy - \frac{h(xy+a)}{h'(a)}}{x^2} dx^2 \right], \quad (9)$$

h being the same function as before (but cf. also the alternative approach of Sec. 5, Eqs. (31–33)). Note that the chart (9) is, after a trivial rescaling, still of the form (2), where, however, now the lines of constant $y \propto x^0$ are different from the Killing trajectories and $x \propto x^1$ does not coincide with a Killing flow parameter. Consequently, in contrast to (3) the form (9) allows to cover also simple zeros of the Killing field. Higher order zeros, on the other hand, will turn out to lie always in infinite distance, so they cannot be covered by a smooth coordinate system.³ Since in two dimensions a Killing field vanishing along a line must vanish everywhere, this exhausts all cases.

Finally, if $W(0, X^3)$ in (4) has zeros (we call the corresponding values of X^3 ‘‘critical’’, X_{crit}^3), then one gets additionally the ‘‘deSitter’’ solutions $X^a \equiv 0, X^3 \equiv X_{crit}^3$,

$$De^a = 0, \quad d\omega = -\frac{\partial W}{\partial X^3}(0, X_{crit}^3)\varepsilon, \quad (10)$$

²In the case that D has extrema, a prior gluing of solutions corresponding to successive branches may be necessary.

³Alternatively to this one may argue equally well that the coordinates in the *target* space (of the σ -model formulation of Part I) corresponding to the charts (3,9) provide an atlas of the respective symplectic leaf. The absence of a chart of the type (9) for zeros of h of higher degree is then explained by the fact that in the target space such points constitute independent (pointlike) symplectic leaves, thus giving rise to other independent solutions, namely the deSitter solutions (10).

which have vanishing torsion and constant curvature all over M .⁴ The metric for such a solution can be brought into the form (3), too, with $h(x^0) = \frac{\partial W}{\partial X^3}(0, X_{crit}^3) \cdot [(x^0)^2 + d]$, $d = const$. As remarked in the introduction, the coordinate system underlying (3) is adapted to a Killing direction. In the case of deSitter space the Killing fields form a *three*-dimensional vector space, in which the vector fields ∂_1 corresponding to the different choices $d = -1, 0, 1$ in h are pair-wise independent (for a basis take, e.g., two of them and their Lie bracket).⁵

We conclude this brief review with three specific models comprised in the above formalism (cf. Part I) which will serve as examples in Sec. 6. First the so-called Jackiw-Teitelboim (JT) model of 1+1 (anti)deSitter gravity [9] obtained by the choice $2W := V(X^3) = \Lambda X^3$ in (4):

$$L^{JT} = -\frac{1}{2} \int_M d^2x \sqrt{-\det g} X^3 (R - \Lambda) \quad \Rightarrow \quad h^{JT}(x^0) = C - \frac{\Lambda}{2}(x^0)^2; \quad (11)$$

here X^3 serves as Lagrange multiplier to enforce the field equation $R = \Lambda \equiv const$, while the X^a -fields were used in (4) to ensure torsion zero. In contrast to the deSitter solutions (10) present also in most of the generic models (4), here the fields X^i are not constant all over M (in particular, e.g., $X^3 = x^0$). Consequently in the case of the *JT*-model the fields X^i break the isometry group of the deSitter metric down to a one-dimensional group; therefore, in contrast to d in the function h of (10), here the constant C distinguishes diffeomorphism inequivalent solutions of the field equations.⁶

The potential $W^{R^2} := -(X^3)^2 + \Lambda$, as the second example, leads, upon elimination of the X -coordinates, to the Lagrangian of two-dimensional R^2 -gravity,

$$L^{R^2} = \int_M d^2x \sqrt{-\det g} (R^2/16 + \Lambda) \quad \Rightarrow \quad h^{R^2}(x^0) = -\frac{2}{3}(x^0)^3 + 2\Lambda x^0 + C. \quad (12)$$

As an example for non-trivial torsion, the potential $W^{KV} = -\alpha X_a X^a/2 - (X^3)^2 + \Lambda/\alpha^2$ allows to describe the Katanaev-Volovich model [10]

$$\begin{aligned} L^{KV} &= \int \left[-\frac{1}{4} d\omega \wedge *d\omega - \frac{1}{2\alpha} De^a \wedge *De_a + \frac{\Lambda}{\alpha^2} \varepsilon \right] \Rightarrow \\ h^{KV}(x^0) &= \frac{1}{\alpha} \left\{ Cx^0 - 2(x^0)^2 [(\ln x^0 - 1)^2 + 1 - \Lambda] \right\}. \end{aligned} \quad (13)$$

Here x^0 ranges over \mathbb{R}^+ only. In the latter two models X^3 became proportional to the curvature scalar R on shell, while X^a is a Lagrange multiplier for torsion zero in (12) and proportional to torsion $*De^a$ in (13), respectively.

For more details on these and other models consult Part I [1] and the references given there.

⁴According to (6) these solutions remain to be “deSitter” also in the context of (5). If D has extrema, furthermore, then in some cases there will also arise solutions of constant Φ corresponding to the critical values of D .

⁵As we will find below, the universal covering solutions of 2d deSitter or anti-deSitter space may be described by a ribbon-like conformal diagram. Fig. 9 displays such Penrose diagrams for deSitter space where the Killing lines $x^0 = const$ have been drawn; **J1** corresponds to $d < 0$, **J2** to $d = 0$, and **J3** to $d > 0$.

⁶Note, however, that also for the JT-model there are the “critical” solutions $X^a \equiv 0$, $X^3 \equiv 0$ of the symmetry-unbroken type (10).

3 General Remarks and Extremals

To find the maximal extension of the local solutions (3), we want to exploit the symmetries of this metric. As pointed out already in the introduction (3) allows for a Killing field, namely $\frac{\partial}{\partial x^1}$. The function $h(x^0)$ measures the norm squared of this Killing vector, furthermore. In particular a zero of h indicates that the line $x^0 = \text{const}$ is a light-like (null) Killing trajectory. We will adopt the customary term *Killing horizon* for such lines and *degenerate Killing horizon* if the corresponding zero of h is of higher order (i.e., $h'|_{h=0} = 0$). Also we will call the regions between two zeros (or beyond the first/last zero) *sectors*. Finally, we call a sector *stationary* if the Killing field is timelike there ($h > 0$) and *homogeneous* if it is spacelike ($h < 0$).

The metric (3) allows also for another symmetry, seen best in coordinates

$$r := x^0, \quad t := x^1 + f(x^0) \quad (14)$$

with

$$f(x^0) \equiv \int^{x^0} \frac{du}{h(u)} + \text{const.} \quad (15)$$

These coordinates are well-defined wherever $h \neq 0$ and bring the metric (3) into the generalized Schwarzschild form

$$g = h(r)dt^2 - \frac{1}{h(r)}dr^2, \quad (16)$$

where h is the *same* function as in (3). (16) has the disadvantage of becoming singular at zeros of h , whereas (3) behaves perfectly well there. However, it displays a further independent (discrete) symmetry, namely one under an inversion of the Killing parameter t , $t \leftrightarrow -t$. If $h > 0$, such that the transformation amounts to a time-reversal, then the metric is called *static*, and thus we see that in two dimensions stationary implies static. This comes, however, as no surprise since in two dimensions any vector field is hypersurface-orthogonal.⁷ In connection with the coordinates (3) this time- (or space-)reversal symmetry will prove to be a powerful tool in constructing the maximal extension. Therefore we write it down explicitly also in the original x^0, x^1 -coordinates:

$$\tilde{x}^0 = x^0, \quad \tilde{x}^1 = -x^1 - 2f(x^0) \quad (17)$$

with f as in (15). Of course, this symmetry works only within one sector at a time, because on its edges (zero of h) f diverges. We will call this transformation *flip*. Note that changing the constant in f yields a different transformation (shifting the origin of the Killing-parameter t and thus the reflexion axis), so actually one has a one-parameter family of flip-transformations. The effect of this flip transformation on the dynamical fields is exactly that of the gauge changing transformation Eq. (61) in Part I. Thus the flip is in fact a symmetry transformation for the full solution to the models (4) or (5).

The standard method for constructing the maximal extension involves the determination of the extremals and the study of their completeness properties. Since we will directly

⁷A static metric can also be characterized by the condition that the timelike Killing field be hypersurface-orthogonal.

apply the transformation (17) to extend our local solutions, this is not really necessary in the present case. Still let us solve their equation for illustrative purposes; after all, extremals, i.e. curves extremizing the action $m \int ds^2$, are supposed to describe the motion of a test particle in the curved background and are used to study the completeness properties of the solutions.

Using the Christoffel symbols $\Gamma_{\mu\nu\rho} \equiv (g_{\mu\nu,\rho} + g_{\rho\mu,\nu} - g_{\nu\rho,\mu})/2$, the equation for the extremals reads

$$\ddot{x}^\mu + \Gamma^\mu_{\nu\rho} \dot{x}^\nu \dot{x}^\rho = 0. \quad (18)$$

For the metric (3) this reduces to

$$\ddot{x}^0 = -h' \dot{x}^1 (\dot{x}^0 + \frac{h}{2} \dot{x}^1) \quad , \quad \ddot{x}^1 = \frac{h'}{2} (\dot{x}^1)^2, \quad (19)$$

with $h' \equiv dh(x^0)/dx^0$. Up to affine transformations, Eq. (18) yields a unique parametrization of the solutions $x(\tau)$. For non-null extremals the arclength s itself is such an *affine parameter*. Let us remark that in the torsion-free case extremals coincide with autoparallels, satisfying $\nabla_{\dot{x}} \dot{x} = 0$, while in the case of nonvanishing torsion they are autoparallel only with respect to the Levi-Civita connection.

Clearly in two dimensions any null-line $g(\dot{x}, \dot{x}) = 0$ solves (18,19). In the chart (3) these *null extremals* are:

$$x^1 = \text{const}, \quad (20)$$

$$\frac{dx^1}{dx^0} = -\frac{2}{h} \quad , \quad \text{wherever } h(x^0) \neq 0, \quad (21)$$

$$x^0 = \text{const}, \quad \text{if } h(x^0) = 0. \quad (22)$$

The extremals (22) are exactly the Killing horizons mentioned above. Plugging these solutions back into (19), we see that for (20) and (21) the affine parameter is $\tau = ax^0 + b$, ($a, b = \text{const}$). Thus these null extremals are complete at the boundaries, iff the coordinate x^0 extends to infinity into both directions of the charts (3). For the models under study this is the case e.g. for all torsionless theories, whereas the KV-model (13) provides an example of incomplete extremals (20, 21) at $x^0 = 0$ (which is still a true singularity as $R \propto \alpha X^3 = \ln x^0/\alpha^2$, [1], blows up there). The affine parameter for the extremals (22) depends on the kind of zero of $h(x^0)$: For non-degenerate horizons ($h'(x^0) \neq 0$) we get $\tau = a \exp(-\frac{h'}{2} x^1) + b$, so they are incomplete on one side, whereas degenerate horizons ($h'(x^0) = 0$) are always complete, as then $\tau = ax^1 + b$.

The non-null extremals are found most easily by making use of the constant of motion associated with the Killing field $\frac{\partial}{\partial x^1}$ (cf., e.g., [11]): $g(\frac{\partial}{\partial x^1}, \dot{x}) \equiv \dot{x}^0 + h \dot{x}^1 = \text{const}$ along extremals. Knowing that for non-null extremals we may choose the length as an affine parameter, this equation may be rewritten in the form

$$(dx^0 + h dx^1) = \text{const} \cdot ds = \text{const} \cdot \sqrt{|2dx^0 dx^1 + h(dx^1)^2|}. \quad (23)$$

The resulting quadratic equation has the solutions

$$\frac{dx^1}{dx^0} = \frac{-1 \pm \sqrt{\frac{c}{c - h(x^0)}}}{h(x^0)} \quad , \quad c = \text{const}, \quad (24)$$

$$x^0 = \text{const}, \quad \text{if } h'(x^0) = 0. \quad (25)$$

(24) is meant to hold only when meaningful; the condition in (25) is immediate from (19). The null-extremals (20,21) can be obtained from (24) as the limiting case $c \rightarrow \infty$. Eq. (24), even if it cannot be integrated explicitly, allows for a comprehensive qualitative discussion of the extremals. For brevity we do not go into details here. Let us just point out that under the flip transformation (17) each extremal (24) is mapped onto another one with the same value of c , but with the opposite sign of the square root. Similarly the two types of null extremals (20) and (21) get interchanged. It is straightforward to see that the line element for the extremals (24) is

$$ds = \frac{1}{\sqrt{|c - h(x^0)|}} dx^0, \quad (26)$$

which will be used to determine their completeness properties. The extremals (25), on the other hand, are obviously always complete, since $x^1 \propto s + \text{const}$ ranges over all of \mathbb{R} .

4 Construction of the Building Blocks, Penrose Diagrams

In this and the following section we will derive the general rules of how to find the Penrose diagrams starting from any given metric of the form (3). In section 6 then we will summarize the resulting simple building block principle and apply it to the specific models (11, 12, 13) for illustration.

Let us first assume that h has no zeros. Then the diffeomorphism

$$x^+ = x^1 + 2f(x^0), \quad x^- = x^1 \quad (27)$$

with $f(x^0)$ as before (15) brings the solution into conformally flat form, i.e., the metric in the new coordinates reads $g = h(x^0)dx^+dx^-$. The Killing field $\frac{\partial}{\partial x^1}$ then becomes $\frac{\partial}{\partial x^+} + \frac{\partial}{\partial x^-}$ and the flip transformations (17) are simply the reflexions at any of the lines $x^+ + x^- = \text{const}$.

Now, according to the asymptotic behaviour of h there are three cases to be distinguished: First, the range of f may be all of \mathbb{R} (e.g. for $h \sim (x^0)^{k \leq 1}$ as $x^0 \rightarrow \pm\infty$). Then the image of the diffeomorphism (27) is the whole (x^+, x^-) -coordinate plane. Second, the range of f may be bounded from one side (e.g. for $h \sim (x^0)^{k > 1}$ as $x^0 \rightarrow \pm\infty$). In this case the image is only the half plane⁸ bounded by the line $x^+ - x^- = \lim f$. Finally, f may be bounded from both sides, in which case the image is a ribbon $a < x^+ - x^- < b$.

In order to get the Penrose diagrams we further apply a conformal diffeomorphism like $x^\pm \rightarrow \tan x^\pm$ which maps the solutions into a finite region, and finally we turn the patch 45 degrees (counter-)clockwise for $h (<) > 0$, given our convention that a positive (negative) ds^2 corresponds to a timelike (spacelike) distance.⁹ The three cases then correspond to

⁸This reflects the fact that then in the original (x^0, x^1) -coordinates any of the null extremals (21) has one of type (20), i.e. $x^1 = \text{const}$, as an asymptotic and thus the null-lines (21) do not intersect all of the null-lines (20).

⁹Remember that h measures the norm squared of the Killing field. Thus $h < (>) 0$ corresponds to homogeneous (stationary) spacetimes.

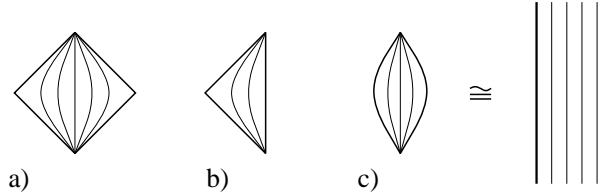


Figure 1: Penrose diagrams for $h > 0$ (thin lines represent Killing-trajectories).

a square, triangle or a lens-shaped region, resp. (cf. Fig. 1; the diagrams for $h < 0$ are similar but turned by 90 degrees). In the last case, however, we will sometimes prefer the (uncompressed) infinite ribbon form.

Let us now come to the cases where h has zeros. These shall be treated by means of a generic example, the function h of which is drawn in Fig. 2a. In Fig. 2b we qualitatively depicted representatives of the null extremals (20, 21, 22) corresponding to the metric of Fig. 2a. Now, within each sector the diffeomorphism (27) could be applied (again exhibiting the flip symmetry of the sector); it, however, breaks down at $h(x^0) = 0$. It may be cumbersome to write down explicitly the diffeomorphism that brings g into conformal form on all of the chart underlying Fig. 2b.

Fortunately, the explicit form of such a diffeomorphism need not be constructed; we can proceed with a simple geometric argumentation: By an x^1 -dependent distortion of the x^0 -coordinate one can straighten the null extremals (21), leaving the horizons (22) as well as the null extremals (20), i.e. $x^1 = x^- = const$, unmodified. Note that in our example the (x^+, x^-) -chart cannot be all of \mathbb{R}^2 any more; rather on the right-hand side there will be some boundary, because due to the asymptotic behaviour of h the null lines of type (21) do not intersect all null lines $x^- = const$. By means of a subsequent conformal diffeomorphism (like $x^- \rightarrow \tan x^-$; cf., however, the following paragraph) and a similar one for x^+ the new coordinate chart covers only a finite region in \mathbb{R}^2 ; the result is drawn qualitatively in Fig. 2c. The boundary on the right-hand side can be made straight by a conformal transformation in x^+ , by means of which one can also transform all rectangles into squares. The final building block for the Penrose diagram is obtained by turning the patch 45 degrees counter-clockwise, as before, and is depicted in Fig. 2d.

In this example all the lines $X^3 \rightarrow \pm\infty$ are complete: The null extremals running there are complete since the coordinate x^0 ranges over all of \mathbb{R} in Fig. 2a (cf. the discussion following Eq. (22)); for the non-null extremals this follows from (26), since $h(x^0) = O((x^0)^2)$. We will draw complete boundary lines boldfaced and incomplete ones as thin solid lines. Horizons are drawn as dashed lines (degenerate horizons, i.e. at higher order zeros of h , as multiply dashed lines); the other null-extremals, which run through the Penrose diagrams under ± 45 degrees, are omitted. Finally, massive dots indicate points at an infinite distance.

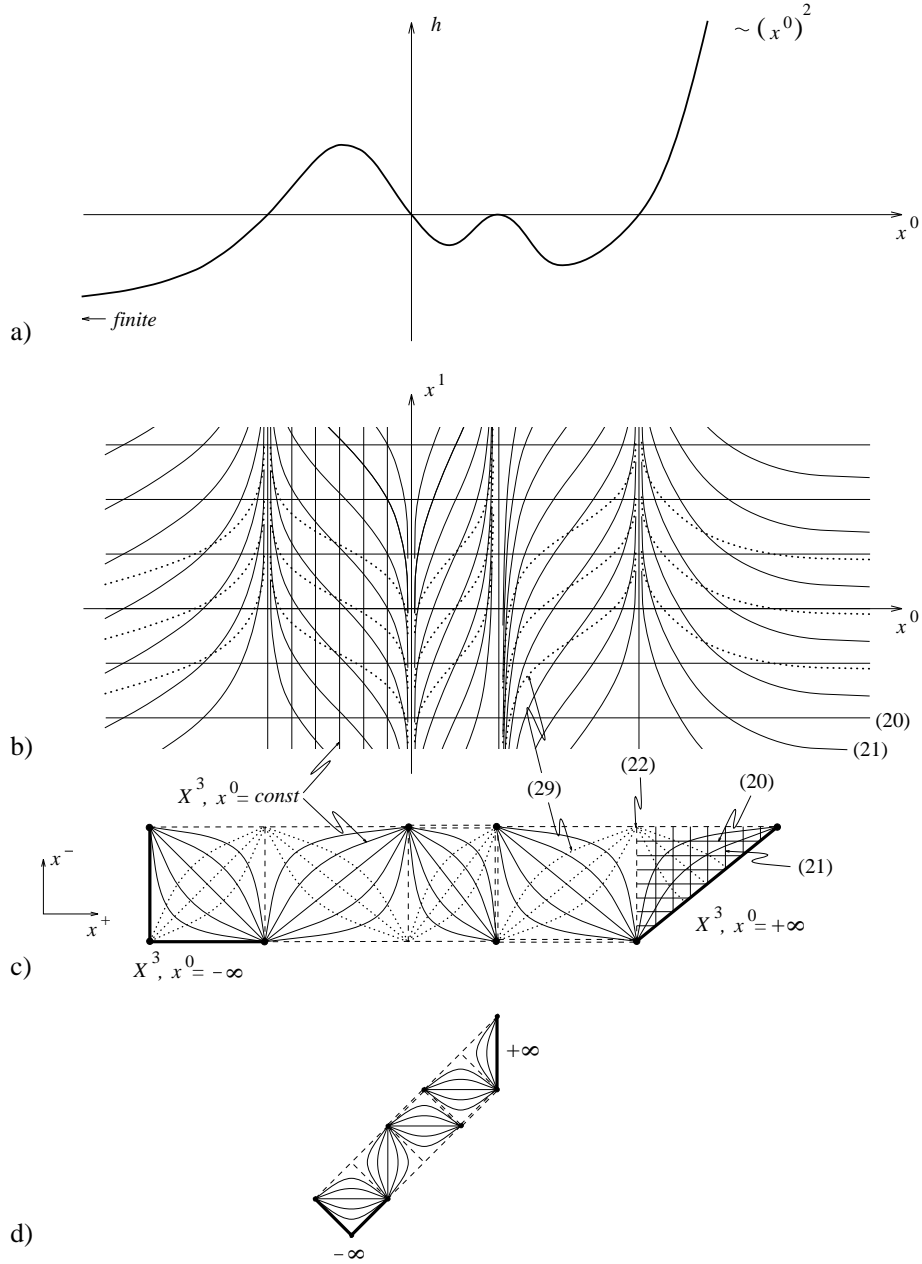


Figure 2: Construction of the fundamental building block for a fictitious function $h(x^0)$. In (b) and part of (c) the null-extremals (20,21) are drawn; in the final building block (d) they would run under ± 45 degrees, but have been omitted. In (c),(d) the horizons (22) have been drawn as dashed lines (degenerate ones as multiply dashed lines). There and in the Penrose diagrams we have also included the Killing trajectories (= lines of constant X^3), which in (b) have been the straight lines $x^0 = \text{const}$, as thin solid lines. The function X^3 , and simultaneously x^0 , increases monotonically throughout the block and the “boundary” values of X^3 are written to the corresponding boundary segments. Finally, in (b),(c) we have drawn the special extremals (29), which are simultaneously the possible flip-axes for the extension, as dotted lines.

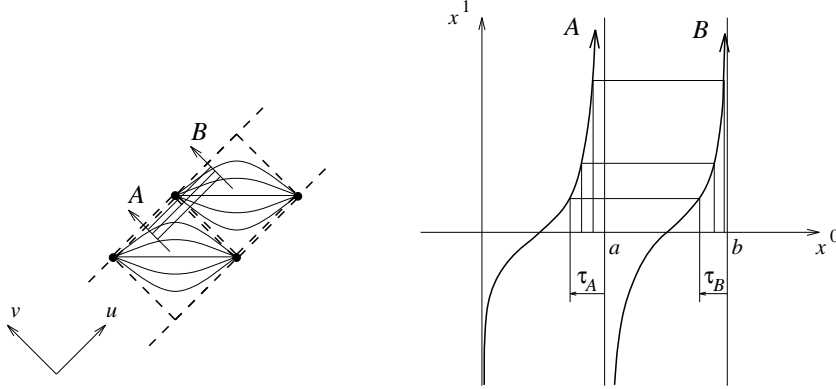


Figure 3: Illustration of relative blue-shift.

As pointed out before, each sector exhibits the flip symmetry. In the example Fig. 2c,d we took this into account by drawing the sectors symmetrically; especially those segments of the boundary depicted as dashed lines are horizons, too, similar to the interior horizons. The solution will thus be extendible at these boundary lines and we must pay attention that the conformal diffeomorphism transforming the x^- -coordinate has the proper asymptotic behaviour to allow a smooth extension. Due to the flip symmetry there is of course a distinguished choice for the x^- -transition function, namely the one making the sector symmetric (this amounts essentially to taking x^- equal to some affine parameter of an $x^+ = \text{const}$ null-extremal). Unfortunately, different sectors may yield contradictory functions, so in general one cannot simultaneously achieve symmetry for all the sectors of the building block.

The situation becomes particularly drastic if $h(x^0)$ has zeros of different order as, e.g., in the example chosen in Fig. 3 (cf. also Fig. 2 and the examples **R3,4**, **G7,10** in Sec. 6): Let A and B be null-extremals leaving the building block across a degenerate (double zero of h) resp. non-degenerate horizon as shown in Fig. 3. In the chart (3) they are described by Eq. (21) and as their affine distance to the horizon we may choose $\tau_A := a - x^0$ and $\tau_B := b - x^0$. The conformity of the building block requires that a chosen spacing along the null-extremal A transfers to the extremal B via the family of perpendicular null-extremals (20), i.e. the lines x^1 or $v = \text{const}$, (cf. Fig. 3). Now, near the horizon the extremal A may be described asymptotically by $x^1 \sim 1/\tau_A$ and B by $x^1 \sim -\ln \tau_B$, hence $\tau_B \sim e^{-1/\tau_A}$. When approaching the horizons τ_A and τ_B vanish simultaneously, but also $\frac{d\tau_B}{d\tau_A} \rightarrow 0$. This already impedes a smooth diagram, which is seen as follows: Choose a conformal gauge (1) and let A and B be represented by $u = \text{const} = u_A$ or u_B , resp. The affine parameter along these null-extremals then satisfies $d\tau_A/dv \propto \exp(\rho(u_A, v))$ and likewise for B , as is easily shown. But from the above we know that at the horizons

$$\frac{d\tau_B}{d\tau_A} = \frac{d\tau_B/dv}{d\tau_A/dv} \propto \frac{\exp(\rho(u_B, v))}{\exp(\rho(u_A, v))} \rightarrow 0. \quad (28)$$

Thus the conformal factor $\exp(\rho(u, v))$ will either diverge along A when approaching the horizon or, if rendered finite along A , vanish along B . It is thus *impossible* to draw a

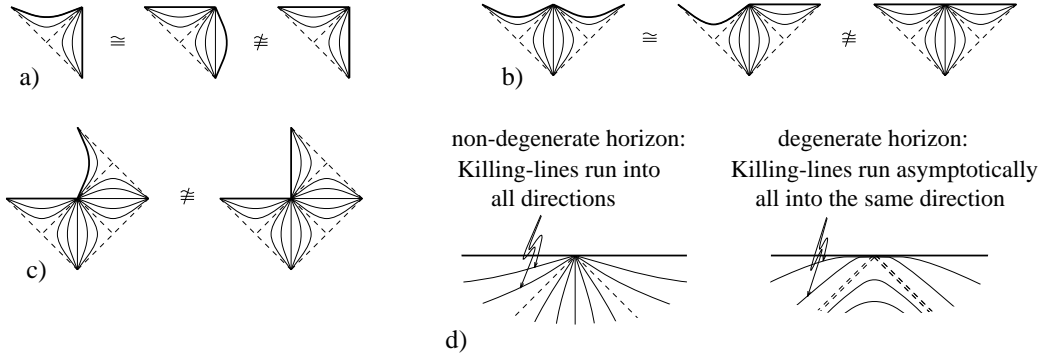


Figure 4: Distorted Penrose-diagrams.

smooth Penrose diagram in this case! A physical consequence of this is that an observer B approaching the horizon, watching A approaching the degenerate horizon (both observers may also be timelike), will notice that A becomes infinitely blue-shifted.¹⁰ Similar problems occur for any combination of different horizons; only if all horizons are of equal degree the diagram will be smooth.

Nevertheless, it is still possible and instructive to use such “non-smooth Penrose diagrams” for book-keeping when constructing the extension and for studying the causal structure. In the illustrations Fig. 11,13 we have marked those non-smooth diagrams with the sign ∇ . At any rate, the extended solutions themselves will be smooth.

But even for only non-degenerate horizons there may occur problems, if two triangular sectors meet. While for *one* sector the boundary can always be made straight by a conformal diffeomorphism, this may be impossible for *two* adjacent sectors simultaneously: Any conformal diffeomorphism (which is a reparametrization of each of the two lightcone-coordinates x^+, x^-) alters the angles between boundary and horizon on both sides of the horizon in the same sense; more precisely, the ratio of the tangents of the respective angles is invariant. For instance, in the situation of Fig. 4a, a conformal diffeomorphism which makes the upper boundary straight must necessarily bulge out the right boundary (at least near the corner point), so the angles of the boundaries against the horizon can never be made equal. This argument is also valid for the (already “extended”) diagram Fig. 4c, and for similar reasons the angle in Fig. 4b cannot be smoothed. At the end of Sec. 5 (cf. Fig. 7) we will show by an example that the distorted diagram is in fact the generic case, if two “triangular” sectors meet.

Finally, for degenerate horizons of equal degree these distortions do not occur; one can always obtain right angles or straight lines. But also the Killing lines behave differently then: As can be shown easily using (3,20,21) they no longer run from the corner point of the sector in all directions; instead they leave the corner point in only one direction asymptotically (tangential to the boundary, if there is one; cf. Fig. 4d). This feature applies also to (4d) extremal Reissner-Nordström with its degenerate horizons, which is

¹⁰More precisely, if A is sending out signals towards B at a constant rate with respect to its affine parameter (proper time), B will receive them with an ever increasing and finally diverging frequency (with respect to its own affine parameter).

in this respect drawn incorrectly in most textbooks (e.g. [12]).

5 Maximal Extension and Saddle-Point Charts

In the previous section we have compressed the coordinate patches (3) into finite building blocks. Now we will investigate whether these blocks have to be extended and how to do so.

Let us again examine the cases without zeros of h first. Their building blocks are drawn in Fig. 1 and they are already inextendible, which is seen as follows: If an extension were possible at all, then it must be possible (also) along the null-infinities (i.e., the 45-degree boundaries of Fig. 1a,b) or along the timelike (for $h > 0$) singularities¹¹ (the vertical resp. curved boundaries in Fig. 1b,c). The extension cannot be possible over a corner point *alone*, since this point then cannot be an interior point of a new local chart.

Now, if x^0 ranges over all of \mathbb{R} , then these boundary lines lie at an infinite distance since x^0 is an affine parameter for the null-extremals (20, 21). Thus they cannot be regular interior points and the solution is inextendible. Note, however, that in general null- and non-null extremals may have different completeness properties! The completeness of the null-extremals depends on the domain of x^0 , whereas the completeness of the other extremals hinges largely on the (asymptotic) behaviour of the function h (cf. Eq. (26)). E.g., the boundaries for the R^2 -model (12) are “null-complete” (as $x^0 \in \mathbb{R}$) but “non-null incomplete” (as $\lim_{x^0 \rightarrow \pm\infty} s = \text{finite}$, cf. (26)). Usually a boundary point is called complete only if *all* extremals running into it are complete. On the other hand, *one* complete extremal is sufficient to make the metric inextendible through that boundary point.

If x^0 does not range over all of \mathbb{R} , then the null-extremals are incomplete and perhaps also the other extremals. However, even then the solution is inextendible, since on these boundaries some physical field (X^3 or some dilaton field) diverges. Of course, if these fields are not taken seriously (or if one drops the restriction $D'(\Phi) \neq 0$), then one might try to extend the function $h(x^0)$ smoothly or analytically beyond its original domain and repeat the analysis with this new h to obtain an extension.

In the case where h has zeros, the discussion above is still valid for the first and the last sector, i.e., an extension is not possible beyond those boundary lines. However, at the other, interior, boundary lines the solutions are extendible and this can be done as follows: Already in Sec. 3 we have introduced the flip transformation (17). In the Penrose diagrams this flip shows up as a reflexion of the sector in question. The reflexion axis, running diagonally through the sector, has to be *transversal* to the Killing lines (i.e. horizontal for stationary sectors and vertical for homogeneous ones; cf. e.g. the dotted lines in Fig. 2c). The flip transformation breaks down at the horizons bounding the sector, because it maps the interior horizons onto exterior ones. We can, however, flip (i.e. reflect) the whole building block and thus obtain an extension beyond the previously “exterior” horizons. The gluing thus amounts to taking the mirror image of the block and patching the corresponding sectors together. This procedure has to be performed at each sector of the first building block and after that also at each sector of the new building

¹¹We will use this term even if the “singularity” turns out to be at an infinite distance.

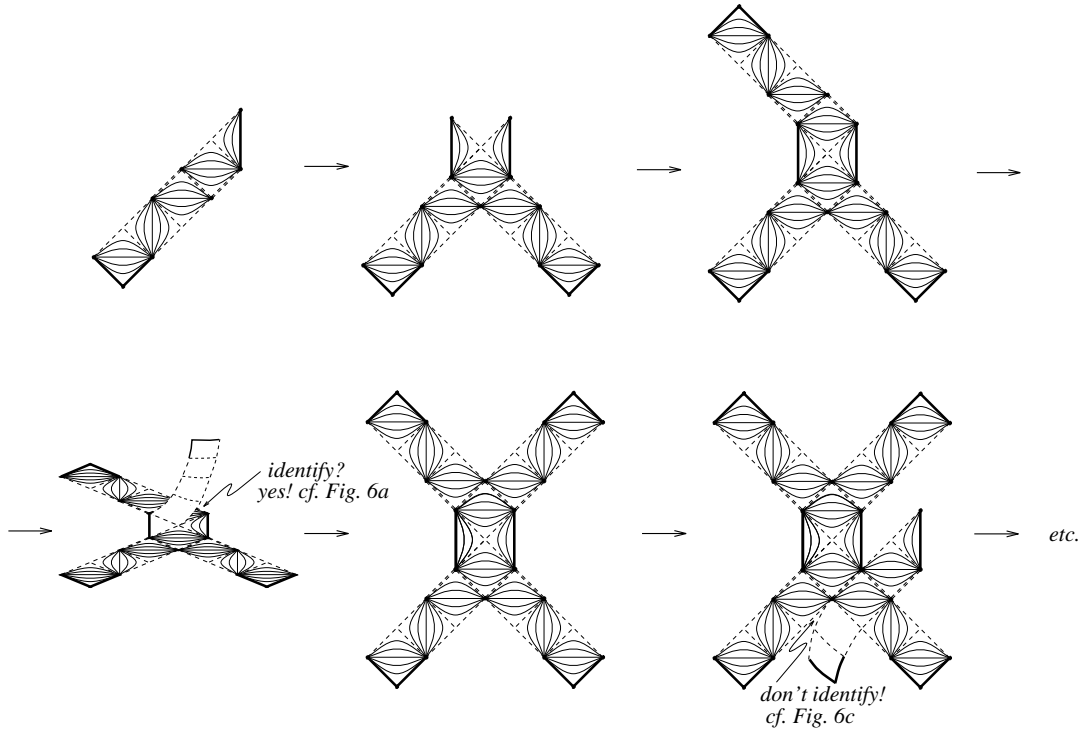


Figure 5: The gluing procedure.

blocks and so on (cf. Fig. 5 for the first steps).

This gluing process is essentially unique; the only free parameter is the choice of the symmetry axis of the flip transformation (i.e. the choice of the constant in (15)), but it only results in a coordinate change (shifting the x^1 -origin of the charts (3)). As long as only the universal covering is pursued this does not affect the solution. However, when further identifications of sectors are made, such that the resulting solution is not simply connected, then we can have an effect of this parameter (this will be discussed in Part III [2]).

We have yet to investigate the case (see Figs. 5,6) that after surrounding the point at the vertex of four blocks the overlapping sectors of the first and the fourth block match. Shall they be identified?

This depends: There is exactly one case where they must be identified (Fig. 6a) and there are a couple of cases where this could (but shall not) be done. A necessary requirement is of course that the sectors are equal (i.e. isometric, scalar curvature and fields like X^3 coincide). This is the case in (a),(d) of Fig. 6, but generically not in (b),(c), because there different sectors overlap (e.g. in (b) the sectors 1 and 5, if numbered consecutively in the building block); only under rare circumstances (e.g. periodic functions h and X^3) they could happen to fit onto one another.

Now to the question whether this shall be done: If the solution *can* be extended smoothly into the vertex point, then of course this must be done, and in this case the overlapping sectors have to be identified to make a single sheet around this vertex point

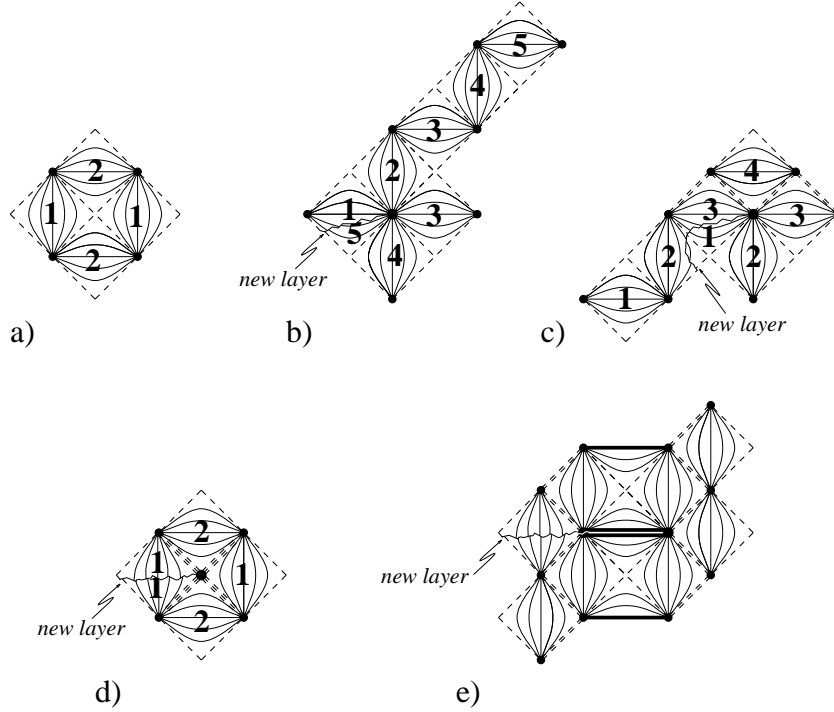


Figure 6: Gluing around a vertex point. Only in (a) the four sectors make up a single sheet around the vertex point. In all other cases (b–d) the vertex point is not an interior point and the solutions must be extended into further new layers covering the original sectors. The same is true for the general situation of e.g. (e), showing part of the extended diagram **G7** (cf. Fig. 13).

(as shown below this will be the case precisely in the situation Fig. 6a). If, on the other hand, the vertex point turns out to lie at an infinite affine distance, then it cannot possibly be an interior point. If under these conditions the sectors were identified, then one would have a non-contractible loop around this vertex point, which cannot be accepted since we intend to construct the (simply connected) universal covering. Thus we must not identify the overlapping sectors but start a “new layer” and continue the gluing, giving rise to the winding-staircase like structure outlined in Fig. 6b–d (cf. also Fig. 11/**R2** or Fig. 13/**G4**). This applies also to the situation (Fig. 6e) that a whole slit is surrounded before overlapping, or even more generally to any occurrence of overlapping sectors different from the arrangement Fig. 6a. On the other hand, if multiply connected solutions are allowed, then an identification of overlapping sectors is possible, certainly. In this case the gluing process is ambiguous, however, and introduces a new geometrically meaningful parameter. Such solutions will be analyzed in full detail in Part III.

Our considerations on the completeness of the horizons (cf. the paragraph below (22)) show already that Fig. 6a is the only candidate for a regular vertex point: Degenerate horizons are complete in both directions, whereas non-deg. horizons are complete on one side only, which is easily recognized as that side of the building block where the Killing lines converge (in Fig. 6 all such complete points have been marked by massive dots). But even the general extremals running towards those vertex points show the same behaviour:

In sectors where the Killing lines run into the vertex point, these extremals are either oscillating ones (between two fixed X^3 - resp. x^0 -values, cf. (24)) or of the kind (25), both of which are complete. In the other sectors, where they have to run transversally to the Killing lines, these extremals are precisely those of (24) with $c = 0$, i.e.,

$$\frac{dx^1}{dx^0} = -\frac{1}{h}, \quad (29)$$

and coincide, furthermore, with the possible symmetry axes for the flip transformations (in Fig. 2b,c we have drawn some of them as dotted lines). Their length follows from (26) where a is the zero of $h(x^0)$ in question:

$$s = \int^a \frac{dx^0}{\sqrt{|h|}} \sim \int^a \frac{dx^0}{(x^0 - a)^{\frac{n}{2}}} \rightarrow \begin{cases} < \infty & n = 1 \\ \infty & n \geq 2 \end{cases}. \quad (30)$$

It is finite only at simple zeros. Thus, whenever a degenerate horizon runs into the vertex point or whenever Killing lines focus there, then this vertex point is at an infinite distance and has to be taken out of consideration. In these cases, to obtain the universal covering we must not identify the overlapping sectors but continue the gluing in a new layer.

In the situation of Fig. 6a (only non-deg. horizons and the Killing lines avoiding the vertex point), however, all extremals are incomplete, and it is to be expected that the vertex point is an interior point of the manifold. This is indeed true: Eq. (9) represents a smooth nondegenerate metric for the neighbourhood of such points, which reveals the vertex point as regular interior point (a saddle point of X^3 , with $X^a = 0$). The four adjacent sectors then constitute one single sheet (cf. also diagrams 3–5 of Fig. 5).

Keeping in mind the Schwarzschild-like form of (16), there is also an alternative way of obtaining such a saddle-point chart, imitating the Kruskal-Szekeres procedure. It was initially proposed by M. Walker [4] for a special rational form of h . We want to show here that it works for *any* sufficiently smooth h (say C^n) with simple zero at $x^0 = a$. The transformation reads (with f as in (15))

$$u = \operatorname{sgn}(h) e^{h'(a) \left[f(x^0) + \frac{x^1}{2} \right]} = \operatorname{sgn}(h) e^{\int \frac{h'(a)}{h(x)} dx + \frac{h'(a)}{2} x^1} \quad (31)$$

$$v = e^{-\frac{h'(a)}{2} x^1}. \quad (32)$$

It brings the metric (3) into the form

$$ds^2 = -\frac{4\tilde{h}(uv)}{h'(a)^2} \frac{dudv}{uv}, \quad (33)$$

which is evidently nonsingular and nondegenerate around $u, v = 0$. Here $\tilde{h}(uv)$ is determined implicitly via $\tilde{h}(uv) = h(x^0(u, v))$. The integration constant hidden in u has to be chosen such that u is continuous at $x^0 = a$.

To show that the transformation (31,32) is really a (local) diffeomorphism consider the following decomposition of the integrand in (31) (separating the singular term):

$$\frac{h'(a)}{h(x)} = \frac{1}{x - a} - \frac{\frac{h(x)}{x-a} - h'(a)}{h(x)}. \quad (34)$$

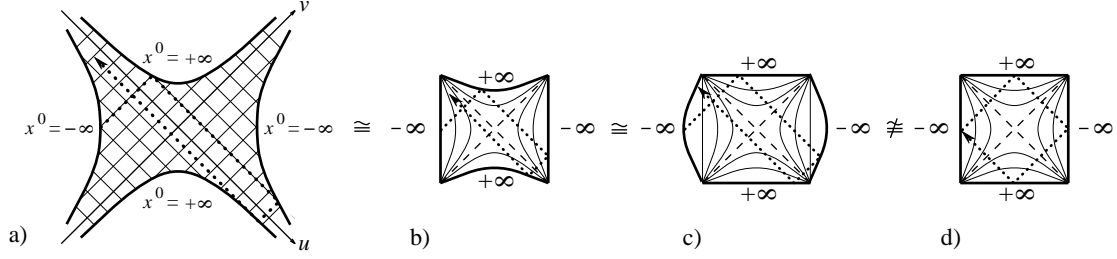


Figure 7: Distorted Penrose-diagrams for the R^2 -model.

The first term yields (after integration and exponentiation) a factor $(x - a)$,¹² and also the second term (being C^{n-2} , if $h \in C^n$) behaves perfectly well. It is thus not at all necessary that h is of the special rational form given in [4, 5].

We are now finally in the position of proving the statement on the distorted boundary of the R^2 -gravity solutions made at the end of Sec. 4. Let e.g. $\Lambda = -\frac{1}{3}$, $C = \frac{4}{3}$, hence (cf. Eq. (12)) $h = \frac{2}{3} [2 - x^0 - (x^0)^3]$. Eqs. (31,32) can be integrated easily to

$$\begin{aligned}
 uv &= \operatorname{sgn}(h) \exp \int_{x^0} \frac{h'(1)}{h(x)} dx = \\
 &= \operatorname{sgn}(h) \sqrt[8]{\frac{(x^0)^2 - 2x^0 + 1}{(x^0)^2 + x^0 + 2}} \exp \left(\frac{-3}{4\sqrt{7}} \arctan \frac{1 + 2x^0}{\sqrt{7}} \right). \quad (35)
 \end{aligned}$$

The singularities lie at $x^0 = \pm\infty$, i.e. at $uv = \exp\left(-\frac{3\pi}{8\sqrt{7}}\right) \approx 1.561$ and $uv = -\exp\left(+\frac{3\pi}{8\sqrt{7}}\right) \approx -0.641$, respectively. The familiar conformal diffeomorphism $u \rightarrow \tan \hat{u}$, $v \rightarrow \tan \hat{v}$ shows immediately that the correct shape of the Penrose diagram must be like in Fig. 7b,c (it is of course possible to straighten the one boundary line at the cost of the other by means of conformal diffeomorphisms). Only if the two hyperbolae $x^0 = \pm\infty$ happen to lie at equal values of $|uv|$ then we can obtain a square. Thus for non-symmetric functions h (with one zero) squares are rather the exception to the rule. This remark applies also to the square shaped Penrose diagrams obtained, e.g., in [5, 13] for other special models covered by the present treatment. Finally we want to mention some physical difference between a world with a square-shaped Penrose diagram and another of the generic form Fig. 7b,c: Only in the former case a series of null-lines “bouncing off” the boundaries closes to a rectangle (cf. dotted lines in Fig. 7).

6 Recipe and Examples

Let us summarize briefly the principle of how to construct the maximally extended Penrose diagram corresponding to any function h in (3) :

¹²Note that the coefficient $h'(a)$ in (31) is absolutely necessary: Otherwise we would have a factor $k \neq 1$ in the singular term, which then integrates to $(x - a)^k$, and the transformation would no longer be a diffeomorphism. This seems to have been ignored in the literature sometimes.

- The number and kind of zeros of the function h determines the number of sectors and their “orientation” in a fundamental building block ($h > 0$ corresponds to stationary sectors, $h < 0$ to homogeneous ones). More explicitly: For n zeros of h there are $n + 1$ sectors in the building block. If a zero of h is of odd order, then the corresponding Killing horizon separates a stationary from a homogeneous sector; otherwise the two neighbouring sectors are clearly of the same type (as h does not change its sign).
- The end sectors of the building block are either a square or a triangle, depending on the asymptotic behaviour of h . It is a triangle, if $f(x^0) = \int^{x^0} du/h(u)$ remains finite at the boundary (e.g., for $h(x^0) \sim (x^0)^{k>1}$ as $x^0 \rightarrow \pm\infty$), and it is a square, if $f(x^0)$ diverges (e.g., for $h(x^0) \sim (x^0)^{k\leq 1}$ as $x^0 \rightarrow \pm\infty$). In the case of a triangle the hypotenuse runs parallel with the Killing lines, of course (i.e. vertical for stationary sectors, horizontal for homogeneous ones).
- Choose any sector and establish the symmetry axis, running diagonally through the sector, transversal to the Killing lines (i.e. horizontal for stationary sectors and vertical for homogeneous ones). Reflect the whole block at this symmetry axis and identify the corresponding sectors.
- Proceed in this way with all sectors until you come to an end, or ad infinitum.
- If after surrounding a vertex point sectors overlap, the Killing horizons running into that point being non-degenerate (simple zero of h), and if the Killing lines do not focus there (Fig. 6a), then identify the overlapping sectors such as to make a single sheet around this vertex point. In all other cases (e.g. higher degree zero of h , Killing-lines running into that point, etc.) do not identify the sectors, but continue gluing in a new layer to get the universal covering.
- Any boundary is null-complete, iff $x^0 \rightarrow \pm\infty$ there. A boundary point is complete with respect to all other extremals (24), iff $\int^{x^0} du/\sqrt{|c-h(u)|}$ diverges there, (cf. Eq. (26)). Complete boundaries have to satisfy both conditions (except that only extremals of one kind run there) and are depicted boldfaced in the present paper.

As pointed out repeatedly before, the Penrose diagrams obtained in this way are to be understood as *schematic* ones only. However, if the zeros of the respective function h are all of the same order, then these diagrams are also smooth; by this we mean that there exists a (smooth) diffeomorphism from the universal covering solution to the respective diagram. Still, if the zeros are all simple (non-degenerate horizons) and two non-null boundary lines meet in a point, then it will in general be necessary to deform the boundary lines somewhat (cf. Figs. 4a–c, 7). For a null and a non-null boundary line meeting¹³ or for higher order zeros these complications do not occur.

If, on the other hand, h has zeros of different degree, then there is *no* smooth diffeomorphism from the universal covering solution to the Penrose diagram; the latter has to be regarded as purely schematic then. An explanation from the physical point of view has been provided by means of a relative red/blue-shift between observers approaching Killing horizons of a different type (cf. Fig. 3). Certainly the universal covering solutions themselves are still smooth everywhere in these cases, too: The gluing diffeomorphism (17) may be used to patch together charts (3) (this poses no problem since only *one* kind

¹³If, say, a spacelike boundary meets a null boundary at a corner point (e.g. in the diagrams **G1-4**, **8,9,11** of Fig. 13), then it is obviously no problem to change the angle of the spacelike boundary at will, since the null boundary always remains null under conformal transformations.

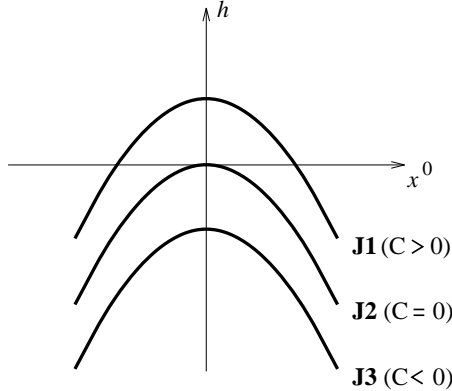


Figure 8: Functions $h(x^0)$ for the JT-model (deSitter gravity).

of Killing horizon at a time is involved) and an atlas is obtained when completing these charts by those of type (9) or (33). Obviously, also in these cases it is instructive to keep track of the patching by a (schematic Penrose) diagram; only it may not be taken as a true smooth image of the respective spacetime then.

We now come to the announced examples, starting with (anti-)deSitter gravity (11). Since all values $\Lambda \neq 0$ yield (basically) equivalent Penrose diagrams, we will set $\Lambda := -2$ in the following. This describes deSitter gravity (note that the sign of the curvature $R \equiv \Lambda$ depends on the signature convention, which in the present paper is different from e.g. [12]). For positive values of Λ (anti-deSitter gravity) the Penrose diagrams obtained below have to be turned by an angle of 90 degrees, while $\Lambda = 0$ yields the diamond like Minkowski space diagrams, of course. With the above choice $\Lambda := -2$ we get a one-parameter family of functions h [cf. Eq. (11)], $h^{JT}(x^0) = C - (x^0)^2$, parametrized by the Casimir constant $C = X_a X^a + (X^3)^2$ (cf. Fig. 8), which leads to the following three qualitatively distinct cases:

J1: For any $C > 0$ $h(x^0)$ has two simple zeros, leading to one square within the fundamental building block. Asymptotically we have $h \sim -(x^0)^2$, so that adjacent to the square there will be a triangle at each side, the boundary of which, $X^3 = \pm\infty$ resp., is spacelike and complete. Gluing leads to the ribbon-like diagram shown in Fig. 9. (For the other sign of the cosmological constant, e.g. $\Lambda = +2$, we get the same diagram for $C < 0$, rotated, however, by 90 degrees, as the boundary is timelike then).

J2: For $C = 0$ we get no square, but only two triangles. The corresponding Penrose diagram is again plotted in Fig. 9.

J3: For $C < 0$ the function h has no zeros (Fig. 8). We therefore may apply directly the diffeomorphism (27) with the function (15), which in the present case can be written in terms of elementary functions:

$$f(x^0) = -\frac{2}{\sqrt{-C}} \arctan\left(\frac{x^0}{\sqrt{-C}}\right). \quad (36)$$

The resulting region (x^+, x^-) is again a ribbon (Fig. 9); but this time without such a

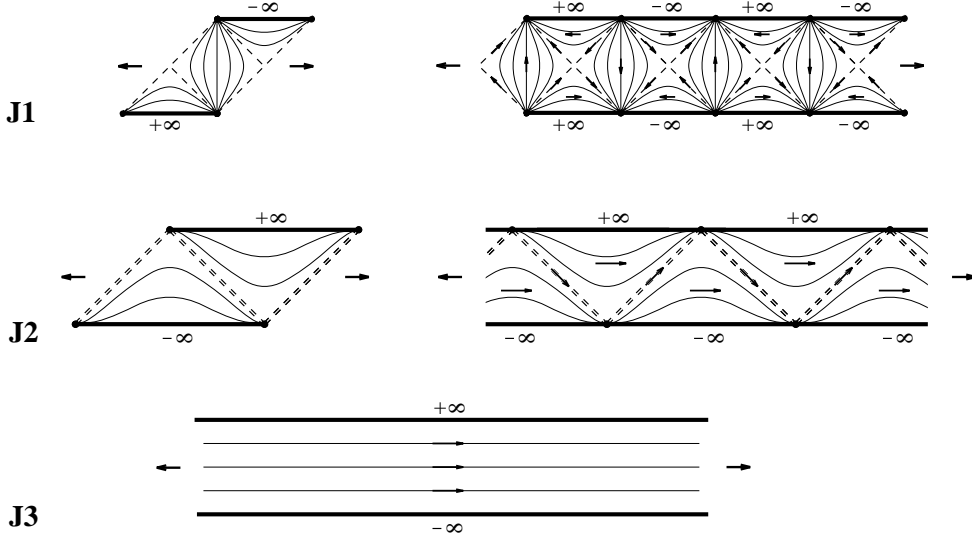


Figure 9: Penrose diagrams for the JT-model; left the building blocks, right the extended diagrams. Arrows inside the diagrams indicate Killing fields for those solutions.

periodic internal structure as before, since the Killing lines $X^3 = x^0 = \text{const}$ become the parallels $x^+ - x^- = \text{const}$ in the present case.

Clearly, as manifolds the solutions **J1-3** are all the same, namely the unique (simply connected, maximally extended) manifold with zero torsion and constant curvature ($R \equiv \Lambda$, cf. Eq. (11)). The difference between the spacetimes **J1-3** arises only from the function X^3 defined on them. As mentioned already in Sec. 2, preservation of X^3 reduces the originally three independent Killing-fields to only one symmetry direction (indicated by arrows in Fig. 9).

Note that while the Penrose diagrams for anti-deSitter space look the same in any spacetime-dimension D (vertical ribbon), this is not the case for deSitter. There a ribbon-like structure appears for $D = 2$ only. This may be understood as follows: D -dimensional deSitter space can be obtained from restricting a $D + 1$ -dimensional Minkowski metric to the one-sheet hyperboloid, the topology of which is $\mathbb{R} \times S^{D-1}$. For $D > 2$ this hyperboloid is simply connected and thus it provides already the universal covering space. Upon spherical reduction its Penrose diagram is the familiar square [12, 11].¹⁴ For $D = 2$, on the other hand, this hyperboloid is topologically a cylinder $\mathbb{R} \times S^1$ and the universal covering, obtained by unwrapping the S^1 to \mathbb{R} , is the horizontal ribbon of Fig. 9. In comparison, to obtain a D -dimensional anti-deSitter metric, one starts from the unit hyperboloid in $\mathbb{R}^{2,D-1}$. This hypersurface has topology $S^1 \times \mathbb{R}^{D-1}$ and the (timelike) S^1 has to be unwrapped for *any* dimension D , leading to the vertical ribbon diagram. Concluding we

¹⁴Precisely: After some transformations $g = \frac{\text{const}}{\sin^2 t} [dt^2 - d\Omega_{D-1}^2]$ (globally), where $d\Omega_{D-1}^2$ is the standard metric on the $D - 1$ -sphere. Extracting also the “latitude” χ of the S^{D-1} , $d\Omega_{D-1}^2 = d\chi^2 + \cos^2 \chi d\Omega_{D-2}^2$, the space can be described as an S^{D-2} -bundle over the square $t \in (0, \pi)$, $\chi \in [-\frac{\pi}{2}, \frac{\pi}{2}]$. Note that the boundary lines $\chi = \pm \frac{\pi}{2}$ of this square are actually internal lines of the manifold (corresponding to the time-evolved North- and South-Pole of the S^{D-1}).

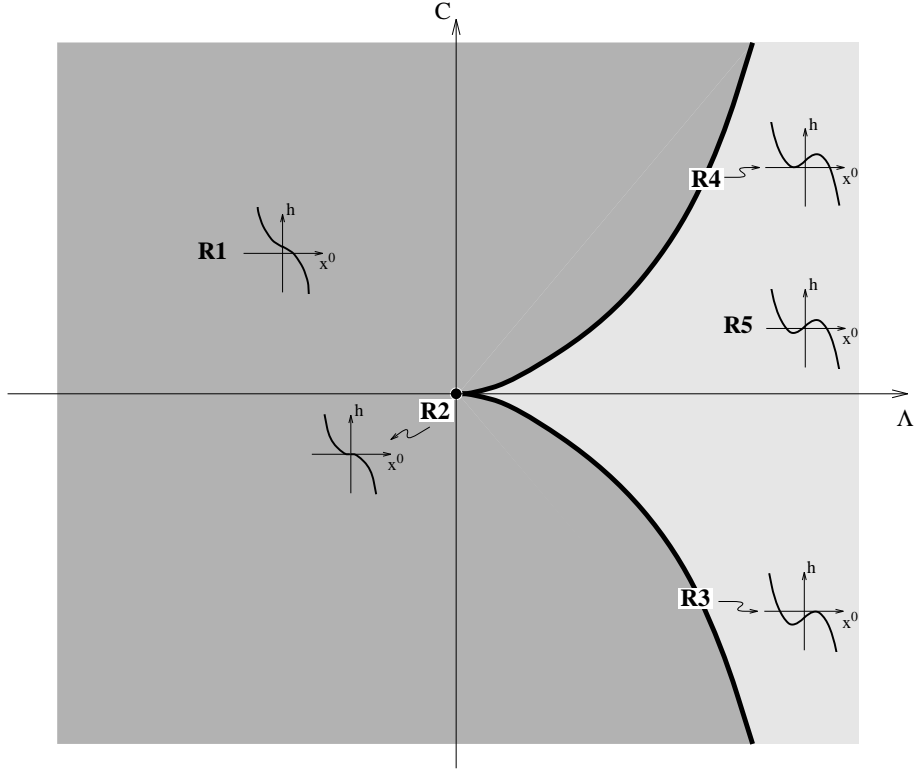


Figure 10: R^2 -gravity, overview.

also observe that for $D = 2$ (and only there) deSitter and anti-deSitter space are related by a simple signature change and the corresponding Penrose diagrams are just rotated by 90 degrees against one another.

Finally, it is of course possible to map the above infinite ribbons into a finite region by a further conformal transformation. For anti-deSitter space this leads for instance to the lens-like form of Fig. 1c and for deSitter analogously to a horizontal lens. However, the periodicity of e.g. the solutions **J1,2** is less obvious in this representation. This remark is also valid for the other infinitely (periodically) extended diagrams to be encountered below (cf. Figs. 11,13,14). In some of those cases (e.g. **R3-5**, **G7,11**) it is even possible to get rid of the multilayered structure, at the cost of introducing a fractal boundary (roughly speaking, the overlapping sheets can be “compressed” into smaller non-overlapping patches).

Let us now turn to the second example: R^2 -gravity (12). The corresponding function $h(x^0)$ is in this case [cf. Eq. (12)] $h^{R^2} = -\frac{2}{3}(x^0)^3 + 2\Lambda x^0 + C$. Since x^0 ranges over all of \mathbb{R} and at infinity $h \sim (x^0)^3$ we get incomplete (null-complete but non-null-incomplete) triangular sectors at both ends of the building block. The corner points are, however, complete, since only the null extremals (22) run into them. A more detailed analysis yields five qualitatively different cases depending on the parameters C and Λ (see Fig. 10):

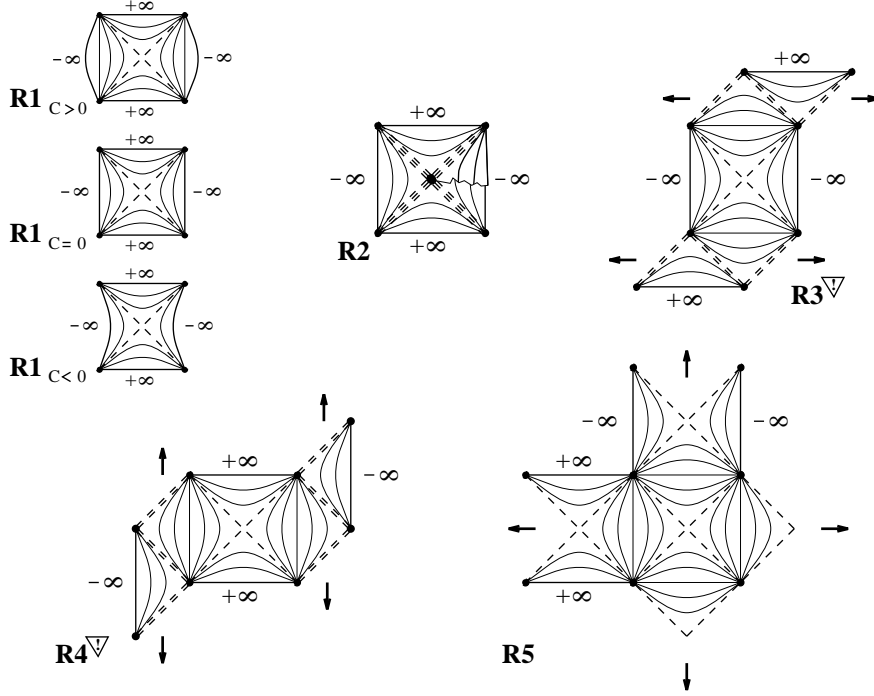


Figure 11: Penrose diagrams for the R^2 -model. Those marked ∇ are non-smooth; furthermore, the singularities of **R5** might be distorted in the same way as sketched in Fig. 4c. (For more details cf. caption of Fig. 13).

- R1** : one simple zero of h at $x^0 = B$
- R2** : one triple zero at 0
- R3** : one simple zero at B_1 and one double zero at $+\sqrt{\Lambda}$
- R4** : one double zero at $-\sqrt{\Lambda}$ and one simple zero at B_3
- R5** : three simple zeros at $B_1, B_2,$ and $B_3,$

where $B_1 < -\sqrt{\Lambda} < B_2 < +\sqrt{\Lambda} < B_3$ and $-\infty < B < +\infty$. Obviously $X^3_{crit} = \pm\sqrt{\Lambda}$ (by its definition as zero of the potential $W(0, X^3)$) and the curve along **R4,2,3** in Fig. 10 corresponds to the critical values $C_{crit} \equiv \pm(4/3)\Lambda^{(3/2)}$ of C . It is completely straightforward to construct the Penrose diagrams according to the above rules. The result is depicted in Fig. 11. Note that not only **R2** but also the extended solutions **R3-5** will be multi-layered; for instance, the copies appended to **R4** at the upper left and the upper right horizon, resp., constitute different layers of the universal covering (cf. Fig. 6e for a similar situation). For non-negative Λ there are, in addition to those diagrams, also infinite ribbons for the constant curvature solutions $d\omega = \mp 2\sqrt{\Lambda}\varepsilon$ (cf. Eq. (10)); in the diagram Fig. 10 they are located at the curve **R4,2,3**, i.e. at $C = C_{crit}(\Lambda)$.

So, for a negative cosmological constant Λ , which in contrast to C is fixed by the choice of the action (12), there is only one schematic Penrose diagram (cf. Fig. 10). The choice of the one free parameter C , however, influences the causal structure of **R1** somewhat, giving rise to the distorted boundaries (cf. also Fig. 7). For positive values of Λ there are mainly two kinds of (again schematic) Penrose diagrams: **R1** and the a bit more

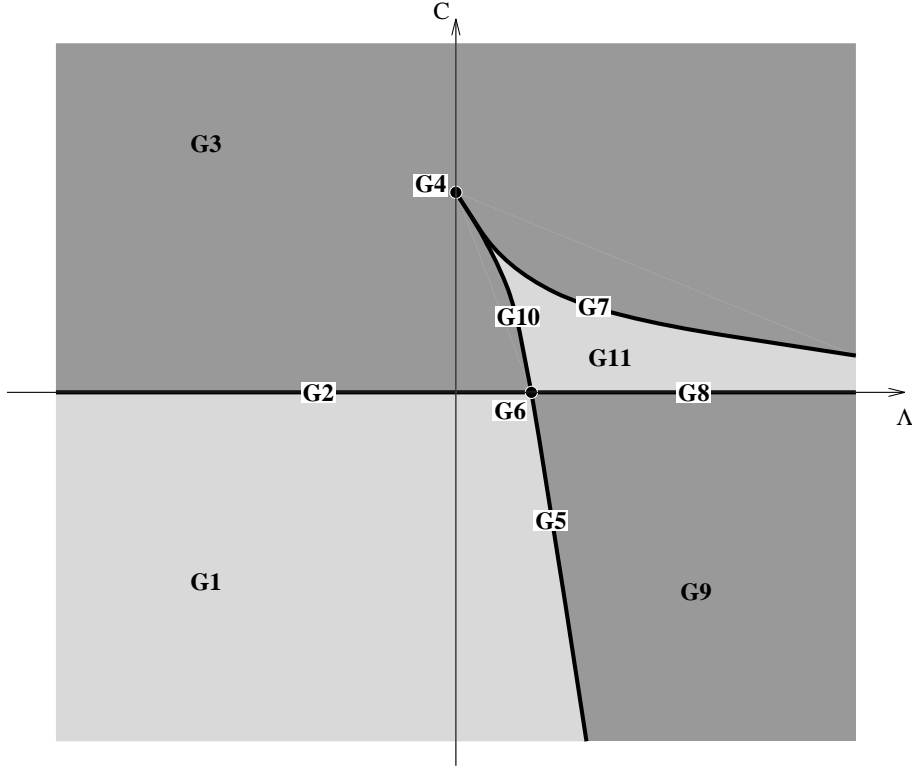


Figure 12: KV-model, overview.

complicated diagram **R5**. Again, to have them smooth, some of the boundaries will be curved for generic values of C (also for **R5**, although this has not been indicated in Fig. 10!). The separation of the solution space into solutions of the type **R1** and **R5** occurs at the values $\pm(4/3)\Lambda^{(3/2)}$ of C . At these values we have the spacetimes corresponding to the (inherently non-smooth) Penrose diagrams **R3,4** and those of deSitter type with $R \equiv \pm 4\sqrt{\Lambda}$ (but now with no internal structure as the functions X^i are constant all over M here). So at $C = C_{crit}$ the Casimir constant does no longer classify the universal coverings uniquely. This is related to the fact that there is more than one symplectic leaf for a critical value of C : Besides a two-dimensional leaf, corresponding to **R4** resp. **R3**, there is the pointlike one $X^+ = X^- = 0$, $X^3 = X_{crit}^3$, corresponding to a deSitter solution of positive resp. negative constant curvature.

The third example is the Katanaev-Volovich model (13). Its function is $h^{KV}(x^0) = \frac{1}{\alpha} \{Cx^0 - 2(x^0)^2[(\ln x^0 - 1)^2 + 1 - \Lambda]\}$, where $x^0 \in \mathbb{R}^+$. The function h^{KV} always has a zero at $x^0 = 0 \Leftrightarrow \alpha X^3 = -\infty$, which is at least of order one. Thus the function $f = \int^{x^0} du/h(u)$ (cf. Eq. (15)) has infinite range as $x^0 \rightarrow 0$, which shows that the Penrose diagrams have a square-shaped sector at this end, the null-infinities, however, being incomplete. On the other boundary of the coordinate patch, $\alpha X^3 = +\infty$, we find $\alpha h \sim (x^0)^2 \ln^2 x^0$, corresponding to a complete triangular sector at this end.

This time we get 11 qualitatively different cases (in addition to two deSitter solutions)

depending on the parameters C and Λ :

- G1,2** : no zeros of h
- G3** : one simple zero at $x^0 = B$
- G4** : one triple zero at $x^0 = 1$
- G5,6** : one double zero at $x^0 = e^{\sqrt{\Lambda}}$
- G7** : one double zero at $e^{-\sqrt{\Lambda}}$ and one simple zero at B_1
- G8,9** : two simple zeros at B_2 and B_1
- G10** : one simple zero at B_3 and one double zero at $e^{\sqrt{\Lambda}}$
- G11** : three simple zeros at B_3 , B_2 , and B_1 ,

where $0 < B_3 < -\sqrt{\Lambda} < B_2 < +\sqrt{\Lambda} < B_1$ and $B \in \mathbb{R}^+$. An overview is provided by Fig. 12. In the above list we took $x^0 \in \mathbb{R}^+$. The cases **G2,6,8** and **G1,5,9**, respectively, differ only in the asymptotic behaviour of h at $x^0 \rightarrow 0$ ($h^{KV} \sim x^0$ for $C \neq 0$, but $h^{KV} \sim (x^0 \ln x^0)^2$ for $C = 0$), which influences the completeness properties (see below). The critical values of X^3 are easily determined to be $\pm\sqrt{\Lambda}/\alpha$; the corresponding value of the Casimir function C is

$$C_{crit} = -4 \left(\pm\sqrt{\Lambda} - 1 \right) \exp \left(\pm\sqrt{\Lambda} \right), \quad (37)$$

which marks the curve **G5,6,10,4,7** of Fig. 12 and simultaneously the deSitter solutions $De^a = 0$, $d\omega = \pm\frac{2}{\alpha}\sqrt{\Lambda}\varepsilon$ (cf. Eq. (10)).

It is now straightforward to draw the Penrose diagrams of the KV-model. The result for $\alpha > 0$ is depicted in Fig. 13 (extended versions of **G5,9** are given in Fig. 14); the diagrams for $\alpha < 0$ are obtained by rotating these by 90 degrees. According to the different behaviour of h at the boundary $x^0 = 0$ the Penrose diagrams **G2,6,8** ($C = 0$) differ from **G1,5,9**, respectively, only by having a complete time-(space-)infinity, $\alpha > (<) 0$, at that boundary (use (26)). Let us stress that all Penrose diagrams in Fig. 13 except for **G7,10** are smooth now, the boundary lines being actually straight (cf. footnote at the beginning of this section). Again, however, a representation of the extended diagrams for **G4,7,10,11** will require infinitely many overlapping layers (cf. Fig. 6e for the case **G7**).

The numbering **G1-11** has been chosen as in [14], where the Penrose diagrams Fig. 13 have been constructed first. It should be noted, however, that our procedure to obtain these diagrams is incomparably faster than the one of [14]. The main reason is that the local solutions used there (resulting also from ours through the diffeomorphism (27)) are valid only in coordinate patches which are part of ours (the sectors $h(x^0) \neq 0$); they had to be glued along their border, which entailed lengthy considerations of the asymptotic behaviour. In the chiral gauge (3), instead, the charts overlap and simply have to be matched together. As a consequence we also could prove that all the solutions of (13), (and in fact also of (4) with an, e.g., analytic potential W) are analytic. As pointed out repeatedly, the Penrose diagrams **G7,10** are, however, not smooth but have to be regarded as schematic diagrams only (of course, the universal covering solutions themselves *are* indeed smooth).

Let us remark that for many of the Penrose diagrams, such as e.g. for **R1, G3,5,9**, it is possible to find also global coordinates displaying explicitly the analyticity of g . E.g., for **R1, G3** we have already found the Kruskal-like coordinates (33) or the more explicit ones (9), and instead of for **G5,9** we provided a global, explicitly analytic chart in a chiral

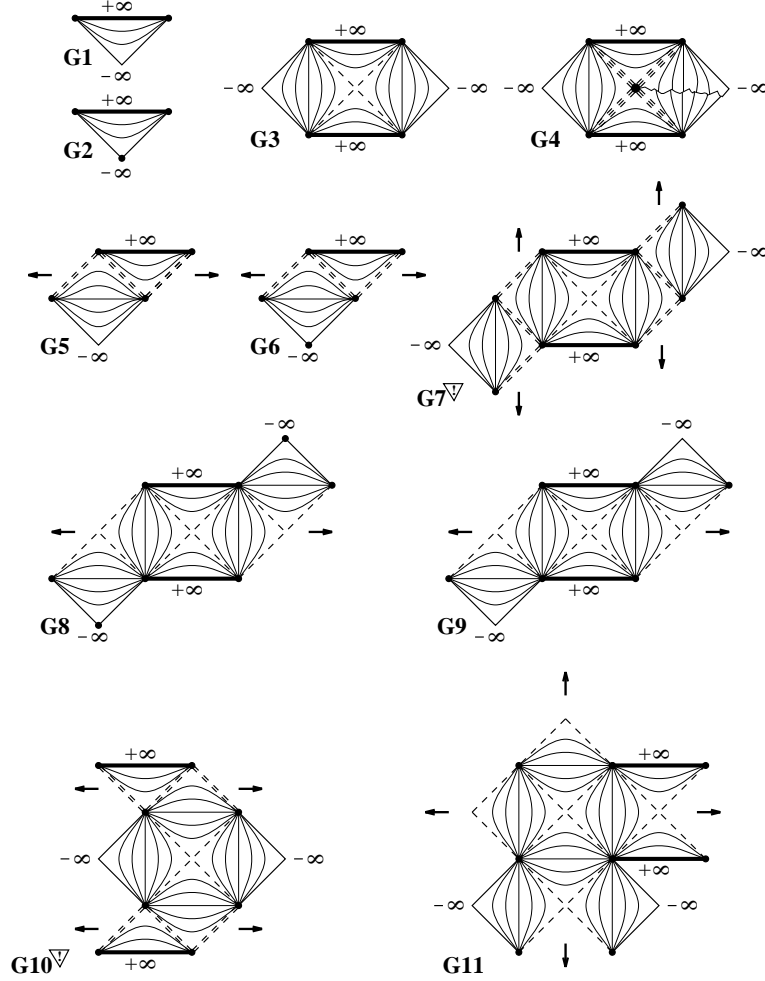


Figure 13: Penrose diagrams for the KV-model (those marked ∇ are non-smooth!). Complete boundary lines are indicated by boldfaced lines, complete points (points at infinity) by massive dots, incomplete boundary lines by thin solid lines, and horizons by dashed lines (degenerate horizons, i.e. at higher order zeros of h , by multiply dashed lines). The null extremals (20, 21) which run through the diagrams under ± 45 degrees are omitted. Arrows outside a diagram (**G5-11**) indicate that the solution should be extended by appending similar copies at the corresponding boundaries (but cf. Fig. 6e).

gauge (2) for the (mathematically) quite similar (four-dimensional) Reissner-Nordström solution in [15]. The method presented there may be adapted easily to cases such as **G5,9** or in fact to any two-dimensional spacetime with a Killing field that allows for a foliation by null-lines.

As a further example for the application of the simple rules outlined at the beginning of this section we could consider, e.g., a model (4) with $Z \equiv 0$ and $W = V(X^3)/2$ where V is chosen to be the derivative of our generic function h in Fig. 2a. In this torsion-free case with, furthermore, $g = 2e^+e^-$ [i.e. without a dilaton-dependent conformal factor, cf.

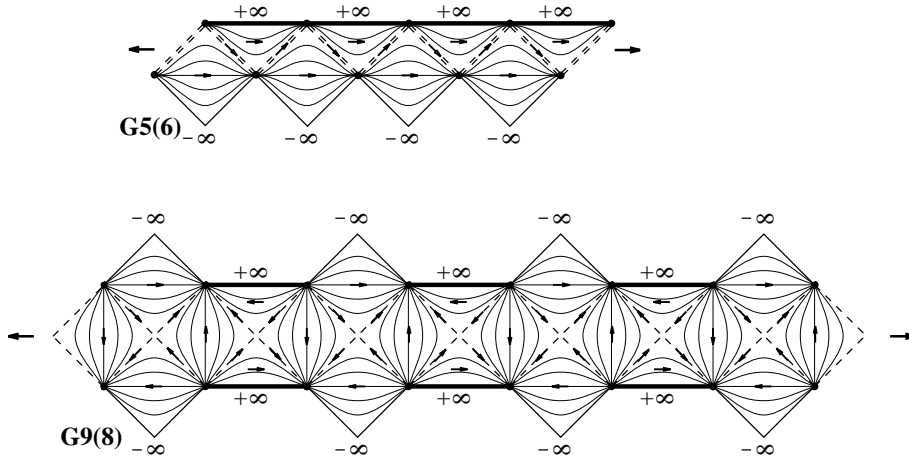


Figure 14: Some extended Penrose diagrams for the KV-model. Arrows inside the diagrams indicate Killing fields.

Eq. (6)], the function h in (3) will coincide with the function in Fig. 2a up to a “vertical” shift according to (7). It is now not difficult to see that there will be 11 qualitatively different schematic Penrose diagrams in this case, as well as further four deSitter solutions (corresponding to the four distinct extrema of the function h in Fig. 2a or, equivalently, to the four zeros of the potential V). We leave it as an exercise for the interested reader to sketch these Penrose diagrams explicitly. Note that some of them will be quite ramified already (cf., e.g., Fig. 5), a feature that becomes more and more pronounced with an increasing number of zeros of V (or h).

7 Final Remarks and Outlook

Starting from the local solutions for the gravity models (4) and (5), we have found all their maximally extended universal covering solutions. They were found to be of an increasing complexity with an increasing number of zeros of the potentials of the Lagrangian. Already in the simpler cases one obtains a diversity of Penrose diagrams as was demonstrated, e.g., in Figs. 11 and 13. The corresponding solution space was found to split into several “phases” as illustrated in Figs. 10 and 12 (where, if $Z := \text{const}$, Λ may be identified also with the “Yang-Mills charge” q , cf. the discussion around Eq. (8)). Let us remark that within figures of the latter type “phase transitions” may be induced by scalar or fermionic matter fields: Given such a matter distribution with a finite support in one null-coordinate on the space-time manifold, the C - and q -values of the matter-free far past will in general be changed into other ones for the matter-free far future (cf. also [8, 16]).

The next step, to be taken in Part III, will be to find all discrete subgroups of the isometry groups of the universal coverings. This task is facilitated substantially by the fact that most solutions have only one continuous symmetry (one Killing field), except for the deSitter solutions, which have a maximal symmetry group (three independent Killing fields). We will be able to classify and parametrize all global, diffeomorphism

inequivalent solutions of arbitrary space-time topology. Here the difference between the various “phases” becomes quite pronounced: For instance, the only maximally extended space-time solution of non-trivial topology with universal covering **G1** (cf. Figs. 12,13) is cylindrical. It will turn out to be a two-parameter solution ($Z \equiv 0$); the second parameter besides C will be found to be an appropriate metric-induced measure for the circumference of the cylinder. A Penrose diagram of the type **G11**, on the other hand, allows, through an identification of opposite horizons in Fig. 13 (cf. arrows), for a spacetime topology of a torus with hole. Extending the diagram further into the vertical direction by some blocks before identifying again all opposite horizons, yields tori with arbitrarily many holes. These (maximally extended) punctured torus solutions are parametrized by $2 + h$ real constants, the geometric origin of which shall be explained in Part III; here h denotes the number of holes ($h \geq 1$). Other identifications lead to punctured Riemann surfaces of higher genera, too. All of them are maximally extended, they have a non-trivial kink number of the light-cone (just follow the movement of the light-cone along a loop enclosing a hole), and the corresponding solution space has a dimension that exceeds the number of generators of the fundamental group of the respective space-time by one.

So, the global structure corresponding to a generic generalized dilaton theory is much richer than that corresponding to ordinary (linear) dilaton gravity or, e.g., spherically reduced vacuum gravity. This richness shows up both in the space-time solutions and in the solution-space (= space of diffeomorphism inequivalent solutions). Therefore, truly generalized dilaton theories allow one to address qualitatively new aspects, e.g.:

- May nontrivial space-time topologies be described on the quantum level, given a quantum theory constructed in a Hamiltonian framework (cf. Part IV) and limited as such to the severely restricted topology-class $\Sigma \times \mathbb{R}$?
- How to quantize a solution-space of a highly non-trivial structure? Or how to resolve the associated difficulties in a Dirac quantization approach (cf. the appearance of “winding numbers” in the quantum states in Part IV)?
- How are the quantum theories for Minkowskian and Euclidean signature of the gravity theories related?

The last of these questions, for instance, is of current interest in the Ashtekar program of 4d quantum gravity [17]. We will find in Part IV that while the spectrum of the ADM mass-operator coincides for both signatures in the case of ordinary dilaton or spherically reduced gravity, there are pronounced differences for other models in our general framework: a continuous ADM mass-spectrum in the Minkowskian version, a discrete or partially discrete one in the Euclidean counterpart.

In an attempt to answer questions of the above kind difficulties arise that are absent in simpler toy-models of gravity. They should be faced, however, in view of the incomparably more challenging task of quantizing full 4d Einstein gravity.

Acknowledgement

We are grateful to H. Balasin, S. Lau, and H. Pelzer for discussions and to H.D. Conradi, H. Kastrup, and W. Kummer for their interest in this work. The work has been supported

in part by the Austrian Fonds zur Förderung der wissenschaftlichen Forschung (FWF), project P10221-PHY.

References

- [1] T. Klösch and T. Strobl, *Class. Quantum Grav.* **13** (1996), 965.
- [2] T. Klösch and T. Strobl, *Classical and Quantum Gravity in 1+1 Dimensions; Part III: All Global Solutions, Part IV: The Quantum Theory*, in preparation.
- [3] J.A. Wolf, *Spaces of Constant Curvature*, McGraw-Hill, 1967.
- [4] M. Walker, *J. Math. Phys.* **11** (1970), 2280.
- [5] D.R. Brill and S.A. Hayward, *Class. Quantum Grav.* **11** (1994), 359.
- [6] T. Banks and M. O’Loughlin, *Nucl. Phys.* **B362** (1991); 649, S.D. Odintsov and I.L. Shapiro, *Phys. Lett.* **B263** (1991), 183.
- [7] M.O. Katanaev, W. Kummer, H. Liebl, *Geometric Interpretation and Classification of Global Solutions in Generalized Dilaton Gravity*, gr-qc/9511009; M. Cadoni and S. Mignemi, *Phys. Lett.* **B358** (1995), 217.
- [8] H. Pelzer and T. Strobl, *Generalized 2d Dilaton Gravity with Fermions*, in preparation.
- [9] C. Teitelboim, *Phys. Lett.* **126B** (1983), 41; R. Jackiw, *1984 Quantum Theory of Gravity*, ed S. Christensen (Bristol: Hilger) p. 403.
- [10] M.O. Katanaev and I.V. Volovich, *Phys. Lett.* **175B** (1986), 413.
- [11] W. Thirring, *Lehrbuch der Mathematischen Physik*, Bd. 1,2, Springer, Wien, New York, 1979; R. Abraham and J.E. Marsden, *Foundations of Mechanics*, Benjamin, New York (2nd Edition), 1981.
- [12] S.W. Hawking and G.F.R. Ellis, *The Large Scale Structure of Space-Time*, Cambridge University Press, 1973.
- [13] J.P.S. Lemos and P.M. Sá, *Phys. Rev.* **D49** (1994), 2897; Erratum, *Phys. Rev.* **D51** (1995), 5967.
- [14] M.O. Katanaev, *J. Math. Phys.* **34** (1993), 700.
- [15] T. Klösch and T. Strobl, *Class. Quantum Grav.* **13** (1996), 1191.
- [16] C.G. Callan, S.B. Giddings, J.A. Harvey, A. Strominger, *Phys. Rev.* **D45/4** (1992), R1005.
- [17] A. Ashtekar, *A Generalized Wick Transform for Gravity*, gr-qc/9511083; *Polymer Geometry at Planck Scale and Quantum Einstein Equations*, hep-th/9601054, (to appear in the Proceedings of GR-14). T. Thiemann, *Reality conditions inducing transforms for quantum gauge field theory and quantum gravity*, gr-qc/9511057.